Proceedings of the 39th IAHR World Congress
19-24 June 2022
Granada, Spain
DOI number

Hydrodynamic Optimization of a large Pumping Station with complex geometry

Sabarots Gerbec Martín[(1)], and Guizzardi Saniago[(1)]

[(1)] Instituto Nacional del Agua, Ezeiza, Argentina
msabger@gmail.com

Abstract

The present work is focused on the study and optimization of the Inlet Pumping Station (IPS) at the Riachuelo System, designed for a 27 m^3/s discharge, with six (out of 8) operative pumps, and a total power of 25MW.

The approach to the study is undertaken by joint numerical and physical modelling. The first is implemented to carry out a preliminary diagnosis of key hydrodynamic aspects and to develop an efficient evaluation of alternatives for the final optimization. The physical modelling is used in parallel to analyze the optimized geometry and to perform a vast range of simulations for different operation scenarios.

A numerical model developed using Computation Fluid Dynamics (CFD) was implemented to diagnose the hydrodynamic behavior of the IPS project under critical scenarios, where high concentrated streams, submerged or surface vortices, flow swirls entering the pump and non-uniform velocity distribution must be limited to achieve an optimal hydraulic performance.

In addition to velocity fields post processed from CFD simulations, vortex core line detection algorithm and swirl angel (SA) were computed to identify undesired hydraulic phenomena. Ratios between SA and vortex detection indicators such as Lambda-2, Q criterion and Helicity, were obtained.

The geometry was primarily optimized to reduce potential sedimentation effects and to limit the swirl angle. Although the swirl angle was reduced by 50% in the optimization process, in 2 suction pipes it results in approximately 8.5º, which is higher than the 7º admissible short-term swirl angle. The swirl angle measured in the physical model was consistently lower than the computed from CFD simulations.

Keywords: Pump Stations; Numerical Modelling; Physical Modelling

1. INTRODUCTION

Water pollution is one of the main problems to the residents within the Matanza-Riachuelo Basin and its surroundings, in Buenos Aires, Argentina. Riachuelo river discharges highly contaminated waters on the Río de la Plata and it is considered one of the most polluted rivers in the world. To ensure health and quality of life of around 4,3 million of residents, the Riachuelo System Project, as a part of the a Master Plan for the decontamination of the most significant urban watershed (Menendez et al, 2011), will provide a primary treatment to the waste waters from highly populated areas.

Figure 1. Riachuelo System Stages

The project is constituted by three stages or sectors (Figure 1). The first sector involves a residential sewerage collector (16,3km long); the second stage consists of an Inlet Pumping Station (IPS), the Pre-treatment Plant (PP) and a second pumping station at the outlet (OPS). Figure 2 shows Stage 2 layout. The last sector of the project considers a 50 m deep shaft, a 10,5 km long tunnel and a diffuser system anchored in the riverbed of Rio de La Plata.

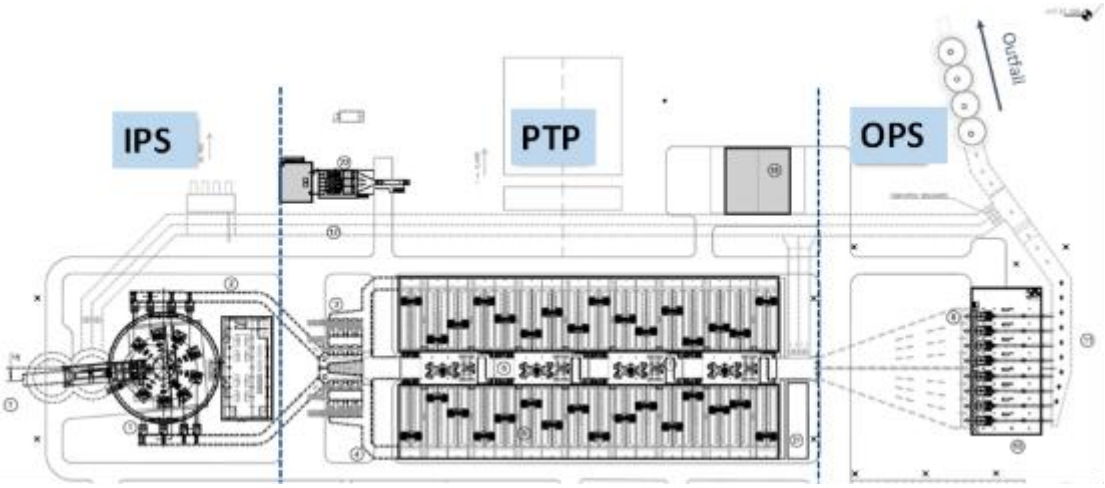

Figure 2. Stage 2 Works Layout

The present paper is focused on the study and optimization of the IPS (Second Stage) designed for a 27m^3/s discharge, with six operative pumps (2 pump as stand-by), and a total power of 25MW.

The IPS can be subdivided into 4 hydraulic structures according to their function and purpose (Figure 3):

- Inlet tunnel: has a circular section of 4.5 m in diameter, with a transition to a square section of 4.5m side. The square section has a development of 20.43 m and has a centerline at of -15.22m .The only purpose of this structure is to conduct the flow into the bottom of the settling chamber that follows.
- Coarse Settling Chamber (CSC): the inlet tunnel flows into a 20.20m diameter x 18m heigh chamber, with a floor of variable dimensions to allow the deposition of large solids in specific places to allow their later extraction. Despite its variability, the bottom elevation is 1.0 m below the inlet tunnel. The main function of the CSC is to provide dissipation conditions and stability of the free surface level and present favorable conditions to settling and deposition of coarse material.

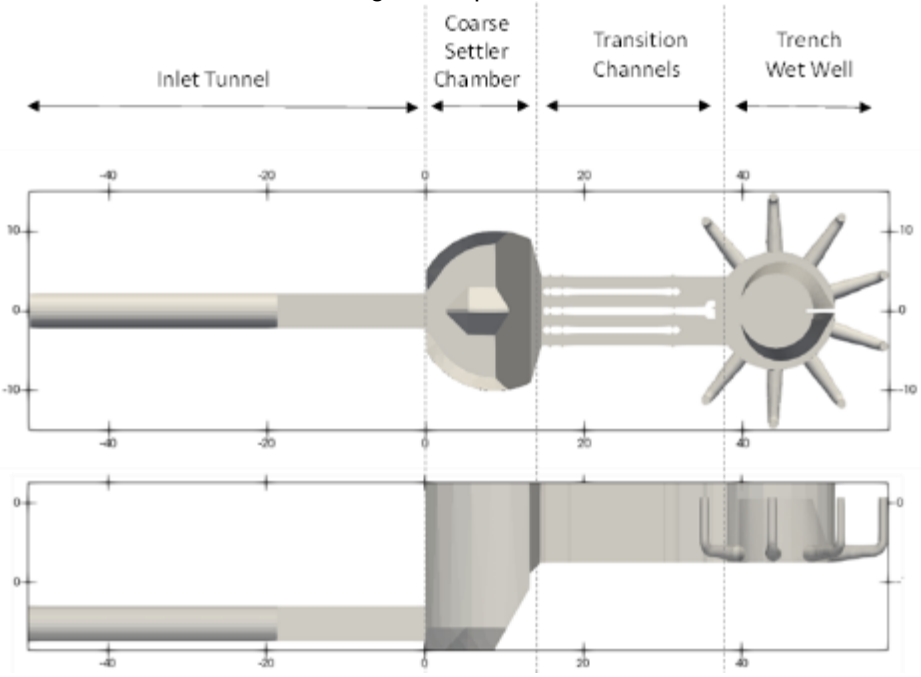

Figure 3. Inlet Pumping Station

- Transition channels (TC): Downstream of the CSC, 10 m above the floor of the inlet tunnel (elevation -7.47 OSN), is a transition of 8.70 m width and 21.7m long. It consists of 4 channels divided by a central partition along the length and two short partitions. The central partition divides the pumping chamber into two and houses, at its end, the gate that allows the two sides of the pump intake to operate separately. Flow distribution in these four channels should be nearly uniform and flow pattern, mainly

in the area approaching the grates, and flow configuration at bulkhead piers must be according to the admissible velocities of the grates.

- Trench Wet Well (TWW): two semicircular channel that feeds the formed suction inlet (FSI), with a converging semi-trapezoidal cross-section. Flow distribution should present symmetry (under symmetrical operation) between the two branches. Meanwhile, the range of velocities should avoid sedimentation, the flow pattern at the FSI, should minimize vortex formation (wall and superficial), maintain reduced rotation and uniform velocities before the pump.

2. MATERIALS AND METHODS

According to the project magnitude, both numerical and physical modelling were implemented to assess the hydraulic behavior of the IPS. In this section, the main characteristics of both approaches are presented.

2.1 Numerical Approach

To study and optimize the IPS, CFD (Computational Fluid Dynamics) type models were built. The public domain open-source code OpenFOAM was used, which numerically solves the Navier Stokes equations on any three-dimensional mesh of polyhedral cells. The simulation is carried out through an implicit iterative scheme, of proven robustness, on the pressure-velocity variables. The code supports parallelization by means of the domain decomposition technique, which allows a considerable reduction in computation time.

The *interFoam* solver was applied for multi-phase flows, in this case water-air, or free surface flow. To ensure convergence to steady state, a visual inspection of the results and the monitoring of total energy series in different sections of the domain is performed, since the solver is essentially transient.

For the treatment of the free surface, a variant of the VOF (Volume-of-Fluid) method was used, which calculates in each cell the volume fraction occupied by the water phase and the air phase, solving the pressure and velocity variables for each phase, considering the viscous effects and the density of each fluid.

2.2 Computational Domain and Boundary Conditions

The modelling domain includes from the inlet tunnel to the 8 FSI. The vertical extension higher than required for the simulated liquid levels, since in addition to the water phase, the air phase is also modelled. In this case, approximately 25% of the modelling domain will be allocated to the air phase.

Four boundary condition were implemented (Figure 4):

- Inlet: a pressure boundary condition is assigned, according to the expected liquid levels in the suction chamber. In the simulations presented in this report, the operating level corresponds to the minimum, N_{min}=-1.64mOSN.
- Atmosphere: for the top patch of the modelling domain, an atmospheric pressure condition is assigned.
- Pumps: for each of the FSI, an outlet flow rate is imposed. Since the operation is with a maximum of 6 pumps and 2 in stand-by, those pumps that are "off" will have a zero output flow value. The flow rate of each pump will be equal and the total will be the maximum operation: Q_{max}=27m^3/s.
- Wall: the rest of the contours of the modelling domain will have a wall boundary condition, where the velocity is zero and the boundary layer development will be conditioned by the smooth wall law implemented in the *software*. (Badano, 2014)

The computational mesh is structured and was generated through *snappyHexMesh*, which intersects an initial basic structured mesh with the surface of the IPS geometry. Refinement areas were implemented where was necessary to achieve a better representation of the flow pattern. The total number of elements is 11.5 million.

2.3 Turbulence models

In pumping station design, it is necessary to characterize the rotational flows near the pump suction, because of the problems that rotational flow induces in the pumps, as high concentrated streams, submerged or surface vortices, flow swirls entering the pump and non-uniform velocity distribution (Elsayed et al, 2020).

Large Scale Simulation (LES) models are most suitable to simulate, although there is a higher computational cost (Škerlava et al, 2011). In order to achieve a correct hydrodynamic representation with high computational efficiency, RANS models have been used as a complement, i.e. to primarily evaluate the global hydrodynamic and initial conditions. Then DES (which combines the LES approach with RANS models to model flows near walls) was implemented to a final assess of the hydrodynamic behavior.

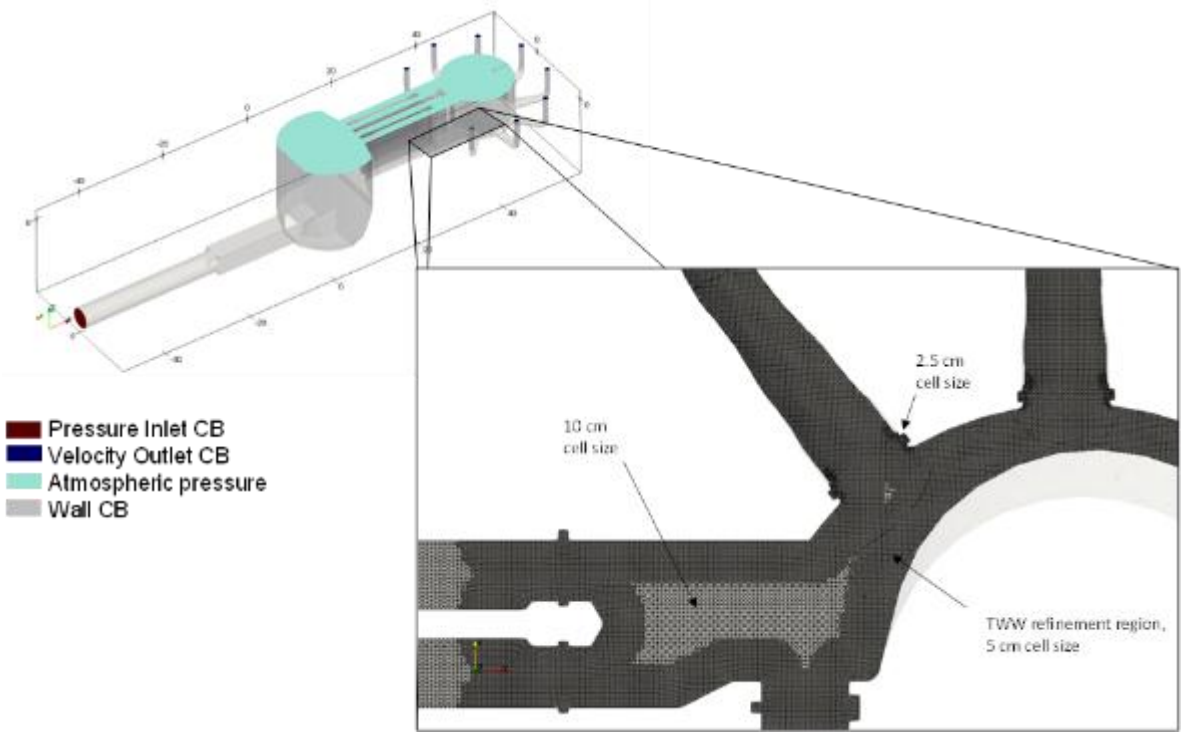

Figure 4. Boundary conditions and mesh refinement

According to best practice, an 80% of the Turbulence Kinetic Spectrum (TKE) should be resolved by the mesh, and the other modelled by the LES turbulence closure model (Gerasimov, 2016). This criterion was successfully verified within the TWW (were the mesh was refined with cell size of 0.050m to 0.025m), while upstream (from the inlet tunnel to the transition channels), the mesh resolves almost 60% of the TKE.

2.4 Physical Model

A 1:10 scale physical model has been built with the same domain as the numerical model (Figure 5). The instrumentation consists of piezometers located at different points of the model, rotameters located in the suction ducts, velocimeters and complementary elements to identify the flow pattern.

Rotameters are placed in the suction pipes of the pumps, allowing the estimation of the rotationality induced by the flow (swirl angle).

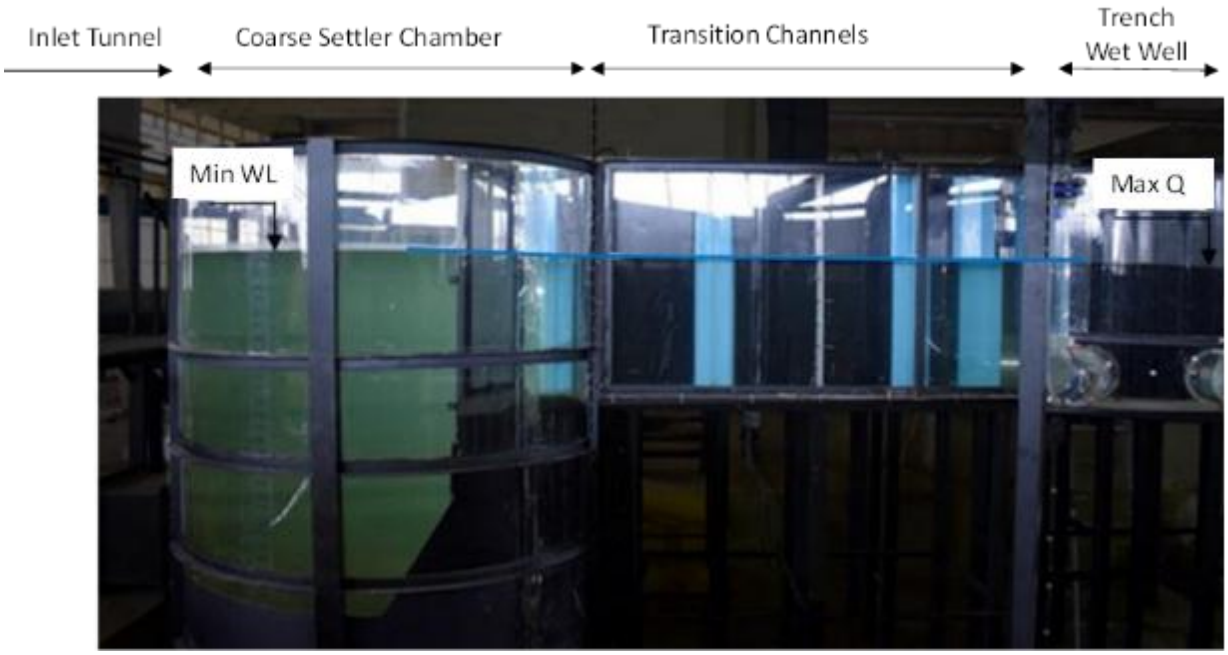

Figure 5. View of the IPS Physical Model (scale 1:10)

There are specific standards that determine the admissible swirl angle limits limits (ANSI/HI, 1198). It is also determined that rotameters must be located four diameters from the pipe vertical downstream of the pump.

In this case, the pumps are located downstream of a horizontal suction pipe and then a vertical elbow provided by the manufacturer. Thus, the rotameter position suggested by the standard cannot be reproduced.
However, the implementation of these instruments provides a reliable indicator of the flow pattern that enters each pumping unit.

3. RESULTS

In this section results of a symmetrical operation at maximum discharge (27 m^3/s) at minimum water level (-1.64mOSN) are presented. First, a global assessment of the hydrodynamics and the verification of CFD results compared to the physical model are shown. Then an optimization is presented.
The main hydraulic structure that required an optimization process was focused on the internal shaping of the convergent semicircular channel of the TWW. The system originally adopted, with a converging channel and a semi-trapezoidal cross-section, gave good results in terms of approaching velocities and swirl angle, but it generated velocities lower than the minimum required to avoid sedimentation processes.

Then, the optimization of the TWW and the flow pattern are evaluated by multiple vortex indicators, included de swirl angle that correspond to the usually used parameter to evaluate the feasibility of pumping stations (ANSI/HI 1998).

3.1 Global assessment

The hydrodynamic of IPS is schematized below (Figure 6). The flow arrives in the CSC where it dissipates energy and flow is rearranged to enter the TC. This involves recirculation effects within the chamber and low velocities. In the transition channels the flow develops towards a uniform condition in the vertical by uniformising its velocity and avoiding flux concentration on the approach to the grates.

Once in the TWW, velocities are verified to be over a certain threshold to avoid sedimentation processes. The flow is then driven into the intakes, which after a short section present a 90º bend towards the pumps positions.

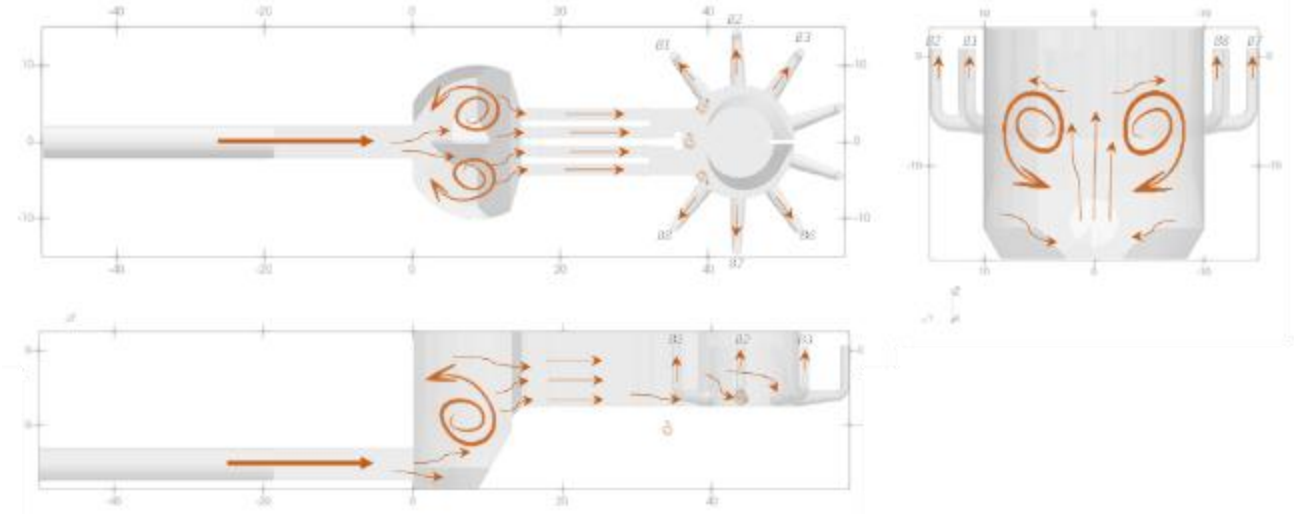

Figure 6. Schematized hydrodynamic of the IPS

From the numerical modelling it was possible to understand the general functioning of the IPS. The CSC shows a superficial recirculation (which is visualized from tracers in both Physical and vectors in the CFD). It is also recorded at depth, with a combination of vertical and horizontal axis circulations and eddies. Figure 7.a. shows a comparative between the superficial velocity field on both physical and numerical models. As can be appreciated from both models, there is an asymmetrical recirculation, despite de symmetrical geometry.

Low velocity re-circulations within the coarse shaft result in velocities compatible with sedimentation, and 72% of the chamber below the IT invert can be computed with velocities less than 0.6 m/s.

The flow separations visually identified as perturbations in the free surface at different locations in the model are clearly captured by the CFD (Figure 7.b).

On the other hand, the low velocities and partial dissipation of energy lead to a rearrangement of the flow towards the intermediate channels, with an acceptably uniform flow distribution between the channels, with deviations of 1.2% with respect to a perfectly distributed flow (Figure 7.c).
The vertical contraction of the flow at the entrance to the transition channels decreases along the path, which can be observed in the velocity profiles recorded by CFD modelling and validated in the physical model (Figure 7.e).

As can be seen in the lateral view, streamlines at Pump 1 come from the lower layer, meanwhile at Pump 2 proceed from an intermediate layer, and finally the flux at Pump 3 is forced from the upper layer. This change in the directions of the flow at the extreme intake, going down at first to then coming into de FSI implies a highly rotation flow induced in this intake.

In relation to the pumping chamber, the original geometry induces a flow towards the pumps with an admissible (measured) swirl angel (less than 3º), but the sedimentation velocities are lower than the admissible ones (Figure 7.f).

It should be noted that the swirl angles (SA) values measured in the physical model are proportionally lower than those processed from the CFD results. In general the ratio is $SA_{physical}/SA_{CFD}$ =0.5. That is, the CFD tends to overestimate the swirl angle. This can partly be explained by the fact that in the CFD model the rotameter is not represented, instead there is a free flow within the FSI. Even though the rotameter is a measuring element whose friction to the angular movement is minimal, a disturbance of the flow generated by the rotameter cannot be neglected. In addition, swirl angle was integrated considering the magnitude of the angular velocity, without considering the rotation sign.

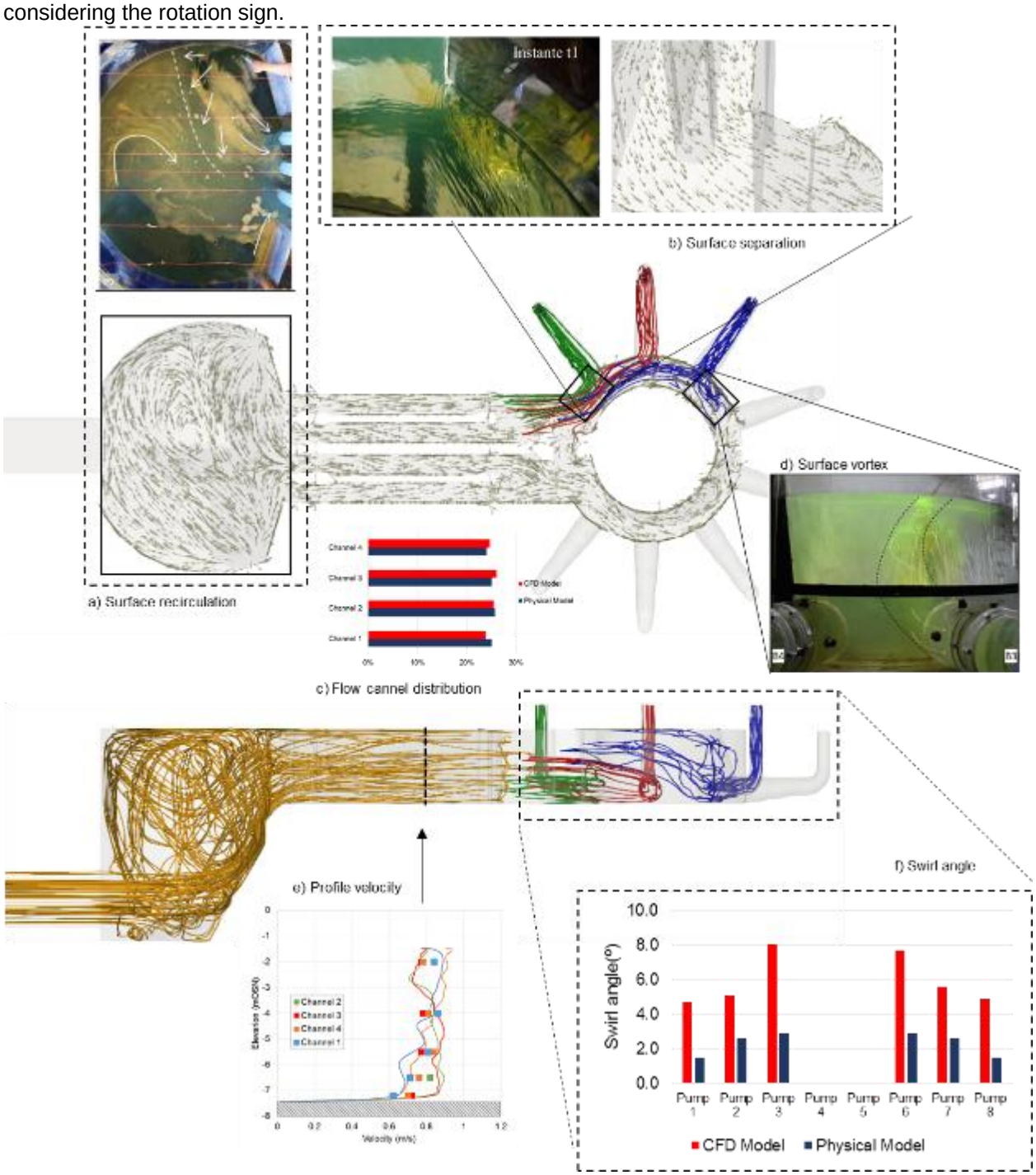

Figure 7. Comparison between CFD and Physical model and IPS global performance

Although the IPS as a whole performs adequately in relation to the design criteria, it is the sedimentation velocity condition in the pumping chamber that implies a revision on the design of this element.

3.2 Optimization

As it has been presented above, even though swirl angle values were admissible at de FSI, velocities in the wet well were lower than the expected. In order to get higher velocities to avoid sedimentation, a reduction of the TWW was tested. The Figure 8 presents the schematized cross section of the left channel to the FSI branch consisting of a trapezoidal section. Alternative A presents a rectangular cross section and Alternative B presents a composite cross section, with a rectangular section below the FSI intake and trapezoidal cross section above the FSI soffit levels.

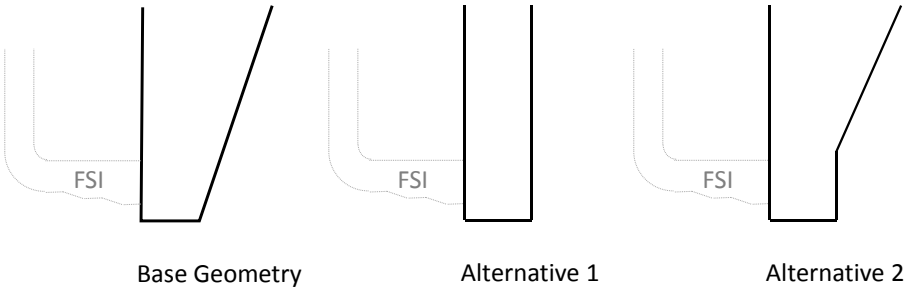

Figure 8. Cross section of different geometries at the left channel of the TWW (dimensions out of scale)

To evaluate the performance of these alternative geometries, velocities were processed from the CFD model to ensure no sedimentation processes take place, and the rotational flow in the FSI is kept within the recommended limits. Figure 9 presents the zones prone to sedimentation within the TWW for the different alternatives. It can be seen that, as expected, the reduction of the section at the bottom increases the flow velocities. While there is an improvement between pumps 1 and 2 and to a lesser extent between 2 and 3, it is only a compromise, as a larger increase in velocities would have resulted in an unacceptable increase in flow rotation within the FSI. It should be noted that the low speeds between pumps 3 and 4 are due to the fact that pump 4 is switched off and does not generate circulation in that section.

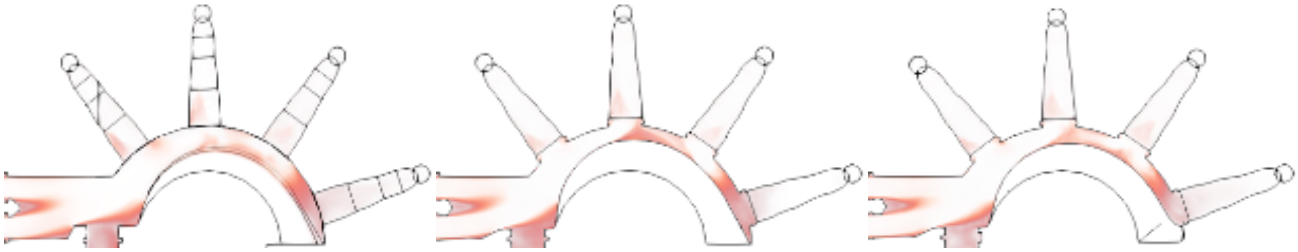

Figure 9. Velocity field below sedimentation threshold (0.6 m/s) at Base geometry (left), Alternative 1 (center) and Alternative 2 (right)

Velocity field is a direct output of a CFD model, meanwhile the rotational flow was evaluated by 4 different indicators: swirl angle: an indicator of the intensity of rotation of the flow (ANSI/HI, 1998), Lambda- 2: an algorithm for the detection of vortex cores. Criterion L-2 determines, for any point in the fluid, whether this point is part of a vortex core (Schafhitzel, 2008), Q-Criteria: where Q > 0 represents the existence of a vortex. The Q criterion defines vortices as areas where the vorticity magnitude is greater than the magnitude of the rate of strain (Jie-min Zhan, 2019), and Helicity: a scalar quantity defined as an inner (dot) product of velocity and vorticity vectors (Gou et al, 2017).

The results for three analyzed geometries of the pumping chamber (Figure 10) are presented below for the SA and vortex indicators. It can be observed that any of the indicators show the higher flow rotation in pumps 3 and 6. In terms of rotation, Alternative 2 presents a similar performance to the Base Geometry. On the other hand, Alternative 1 significantly increases the rotational flow in the end pumps.

The Lambda-2 and Q-Criteria indicators present similar results, while the evaluation of the alternatives by Helicity, although showing that Alternative 2 is better than Alternative 1, does not present as good a performance as the base geometry.

Although the swirl angle was reduced by 50% in the optimization process, in 2 suction pipes it results in approximately 8.5º, which is higher than the 7º admissible short-term swirl angle.

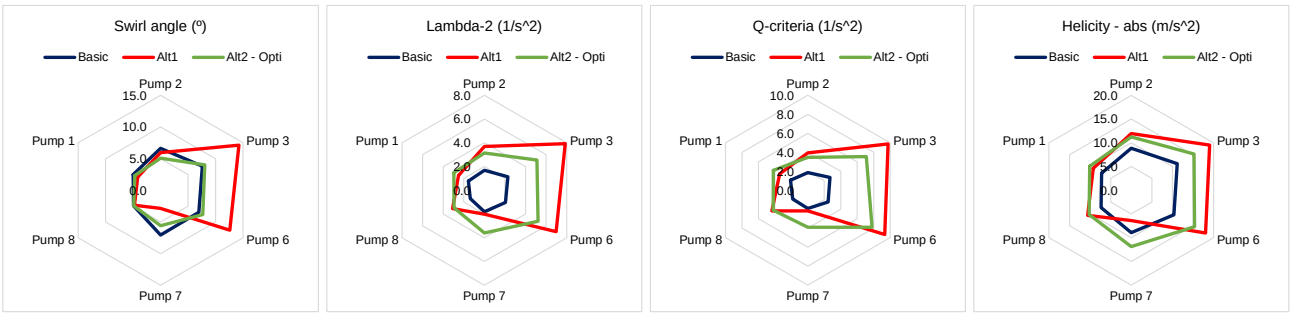

Figure 10. Vortex indicators for each alternative

Further to the simulation of the IPS, an isolated FSI of the Pump 2 was simulated using an uniform inlet boundary condition. Figure 11 shows the marginal effect of the TWW on the rotational flow, where the isosurface of Lambda-2=10 ($1/s^2$) is visualized.

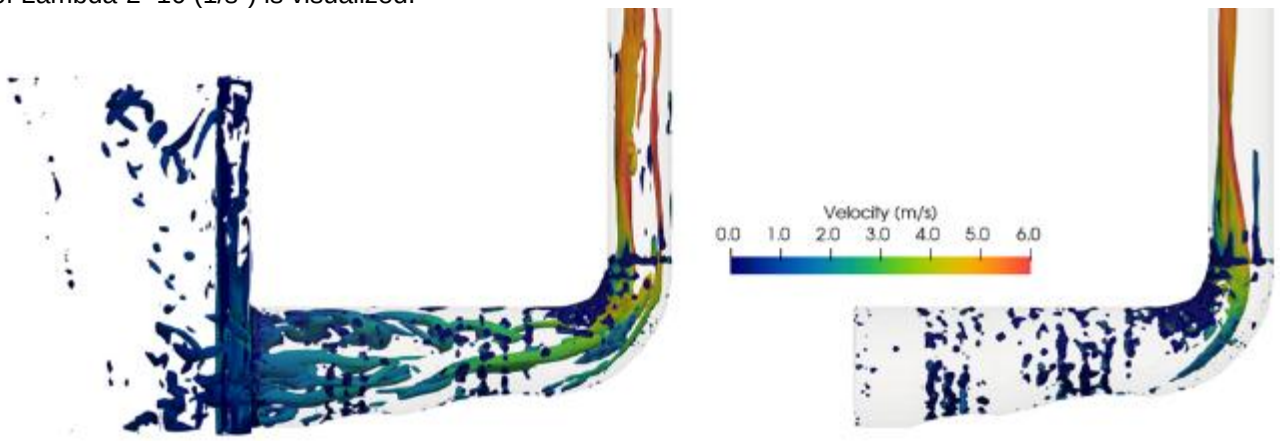

Figure 11. Isosurface of Lambda-a=10: FSI-P2 from the simulation of the IPS (left) and the isolated FSI-P2.

3.3 Discussion

Although swirl angle is the direct indicator taken by the standard to assess flow rotation in the FSI, it is a parameter that implies a prost-processing cost in order to be calculated from the velocity fields.

As an advantage, indicators such as those mentioned (Lambda2, Q and Helicity), are incorporated within the CFD post-processing tools, which provides a flexible/fast tool to evaluate/analyze the flow pattern. On the other hand, they do not have a direct comparison with the standard.

Even though, the correlation between the indicators and the swirl angle is very similar in all three approaches (Figure 12), where the Helicity presents a higher R2.

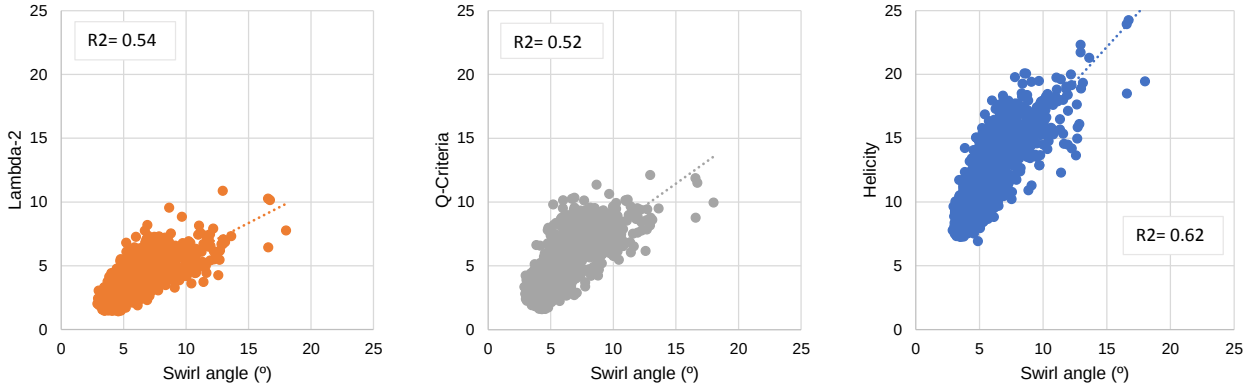

Figure 12. Correlation between swirl angle and different vortex indicators

Then, the correlation between swirl angle and vortex indicators is shown, with the purpose of evaluating if any of these indicators can be complementary to SA and what could be their relationship with the threshold values presented by the Guidance.

Taking into account that the SA values would be overestimating the measurements by a ratio of $SA_{physical}/SA_{CFD}=0.5$ and, being that it is the value measured on the rotameter that is compared with the design parameters of the ANSI/HI standards, the following relationships result between a SA_ANSI/HI=5º and the vortex indicators (Table 1).

Table 1. Range values of vortex indicators according to SA threshold of the standard.

SA_{ANSI}	L2	Q	H
5	4.8 – 6.7	6.7 – 9	15.3 – 18.1
7	6.3 – 9.2	9.2 - 12	18.5 – 22.5

Since a consistent correlation is observed between swirl angle and vortex indicators, it is interesting to obtain relations in surface or submerged vortices classifications. These classifications do not have a quantitative valuation within the norm (as swirl angle does), but the vortex classification criterion is followed (ANSI/HI, 1998). If the vortex indicators could be related to the vortex classification, this would provide an additional processing tool in the CFD to classify vortex and identify possible air entrainment without high computational cost or dynamic mesh refinement (Sabarots Gerbec, 2012).

In addition to indicator processing for a particular section, it is of interest to visualize the Lambda-2, Q-Criteria and Helicity fields in order to identify vortex structures compatible with those visualized in the physical model. Figure 13 shows that both L2 show type 2 surface vortices between pump 3 and 4. The Helicity field, on the other hand, does not show such well-defined structures as the other two indicators. As future tasks, and based on a greater number of tests, the intensity of the L2 and Q fields will be correlated with the classification of these vortices.

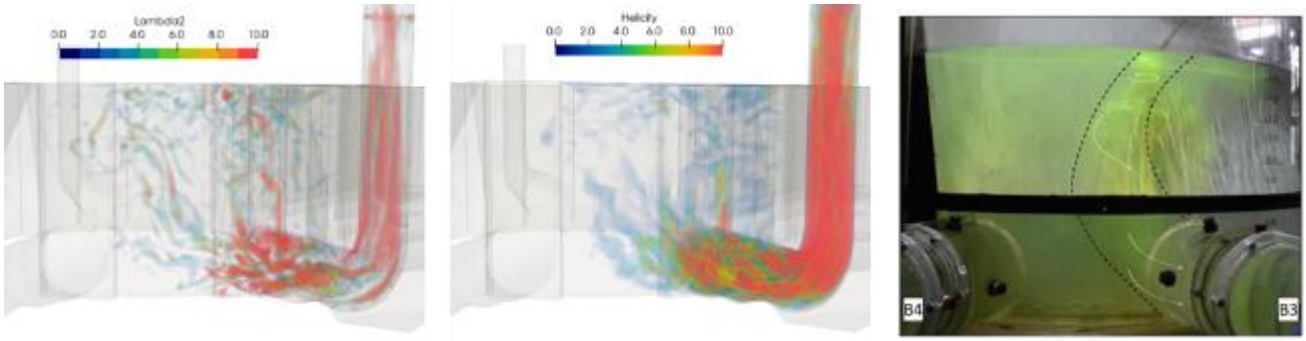

Figure 13. Superficial vortex identification and intensity compared to physical model observation

4. CONCLUSION

Numerical modelling (CFD) proves to be an effective tool in the study and optimization of complex hydraulic problems, as in this case a large pumping station. The support of this methodology with physical modelling provided reliability in the results and facilitates the linking of some parameters with commonly used design standards (in this case the swirl angle).

The optimization concentrated mainly on maintaining admissible swirl angle values without substantially reducing the velocities in the TWW, for which the IPS was improved by changing the section only in the lower layer (below FSI intrados).

It was possible to quantify an overestimation of the swirl angle in the CFD modelling versus to rotameter measurements in the physical model, with an average ratio of $SA_{physical}/SA_{CFD}$ =0.5.

The use of vortex indicators such as Lambda-2, Q-Criteria and Helicity also allows to quantify the rotational flow in the FSI, with a slightly better correlation between swirl angle and Helicity. In all cases the use of the indicators to correlate with the SA values of the standard, there is an error of approximately +/-1º, previously scaling the SA values obtained from the CFD to take into account the overestimation of these values.

The widespread use of these vortex indicators and their relationship to design parameters and vortex classification gives CFD modelling greater utility in the design of pumping stations. In the case of surface vortices, only the L2 and Q indicators showed results consistent with the physical model observations, and an intensity of L2=10 1/s2 would be consistent with a type 2 vortex (Dye core to intake).

5. ACKNOWLEDGEMENTS

Eng. Gastón Latessa for his contributions and insightful comments.

The collaborative work of the Hydraulics Programmed of the Hydraulics Laboratory of the INA, under which the physical model was developed and the measurements presented in this work were carried out.

The technical exchanges and information provided by the Serman y Asoc. staff, in particular by Eng. Nicolás Buono, are a highlight.

6. REFERENCES

ANSI/HI 9.8.(1998) American National Standard for Pump Intake Design. Hydraulic Institute, Parsippany, New Jersey.

Badano, N.D. and Menéndez, A.N., 2014. Evaluación de metodologías para la modelación RANS de la capa límite en conductor circulares. Mecánica Computacional Vol XXXIII, págs. 51-70. San Carlos de Bariloche,

Elsayed G.H., Rabbo M.F.A., Abuzeid M., Elzahry E.F., and Ghanem A. (2020). Study the Parameters Affect on Pump Intake Design Using CFD. *International Journal of Scientific & Engineering Research Volume 11, Issue 10*

Gerasimov,A. (2016) *'Quick Guide to Setting Up LES-type simulations',* ANSYS LES Quick Setup Guide

Guo, Z.W.; Chen F.; Wu, P. F., and Qian, Z. D. (2017) Three-Dimensional Simulation of Air Entrainment in a Sump Pump, J. Hydraul. Eng., 2017, 143(9)

Menéndez A. N., Lopolito M. F., Badano N. D. and Re M. (2011) Influence of Projected Outfalls in the Plata River on Limited Water Use Zones, International Symposium on Outfall Systems, May 15-18, 2011, Mar del Plata, Argentina

Sabarots Gerbec, M., Menéndez A. N. and Badano N., (2012). Modelación hidrodinámica de vórtices superficiales mediante refinamiento dinámico de malla. *MECOM 2012, Salta, Argentina.*

Schafhitzel T. 2008. Topology-Preserving λ2 -based Vortex Core Line Detection for Flow Visualization.

Škerlavaj, A. Škerget, L. Ravnik, J and Lipej, A. (2011). Choice of a Turbulence Model for Pump Intakes. *Proceedings of the Institution of Mechanical Engineers, Part A: Journal of Power and Energy, 225(6), 764–778.*